Influence of oleic acid on the nucleation and growth of 4-N,N-dimethylamino-4-N-methylstilbazoliumtosylate (DAST) crystals

ARTICLE *in* CRYSTENGCOMM · JANUARY 2015

Impact Factor: 3.86

6 AUTHORS, INCLUDING:

Jerald Vijay Ramaclus
Loyola College
18 PUBLICATIONS **32** CITATIONS
SEE PROFILE

F.P. Mena
University of Chile
57 PUBLICATIONS **263** CITATIONS
SEE PROFILE

Edgar Eduardo Mosquera Vargas
University of Chile
26 PUBLICATIONS **35** CITATIONS
SEE PROFILE

Ernest A Michael
University of Chile
45 PUBLICATIONS **243** CITATIONS
SEE PROFILE

CrystEngComm

PAPER

Cite this: *CrystEngComm*, 2015, **17**, 1989

Influence of oleic acid on the nucleation and growth of 4-*N*,*N*-dimethylamino-4-*N*-methyl-stilbazoliumtosylate (DAST) crystals†

Tina Thomas,[a] Jerald V. Ramaclus,*[b] Fausto P. Mena,[b] Edgar Mosquera,[c] P. Sagayaraj[a] and Ernest A. Michael[b]

Received 16th December 2014,
Accepted 20th January 2015

DOI: 10.1039/c4ce02470b

www.rsc.org/crystengcomm

A simple method to control the nucleation and morphology of (4-*N*,*N*-dimethylamino-4-*N*-methyl-stilbazoliumtosylate) DAST crystals is explored. At equal concentrations of oleic acid and DAST in methanol, pure DAST crystals with an irregular hexagonal shape are obtained by a solvent evaporation method. The influence of oleic acid on facilitating the growth in specific faces is investigated. The purity of the grown crystal is investigated by powder XRD, NMR and Raman spectroscopy analyses. As a major improvement, we present a method where a preference for the growth of one of the desired faces (010) in the final morphology of the DAST crystal is possible which would be attractive for terahertz generation and detection studies.

Introduction

The development of technology for the terahertz (THz) spectral range (also known as the sub-millimeter or far-infrared range) is an extremely attractive research field, with interest from sectors as diverse as space and atmospheric sciences, spectroscopy and astronomy, semiconductors and microelectronics, defense and home security, medical and pharmaceutical, manufacturing and material science, as well as agriculture and forensic science.[1] In particular, astronomy and space research have been two of the strongest drivers for THz research and, as a consequence, international projects like the Atacama Large Millimeter/sub-millimeter Array (ALMA) are already operating in Chile. ALMA is considered to be one of the world's largest astronomical projects.[2] Moreover, in 2004, the Massachusetts Institute of Technology, MIT, classified THz technology as one of the ten new technologies that is going to change our lives.[3]

There is a vast array of potential sources of THz waves each with relative advantages, and advances in various research areas continue to provide new candidates.[4] However, high emission power at a low cost for a portable room temperature THz source is the major constraint for future THz systems, which is difficult to achieve due to the fact that the power levels of present electronic and optical devices decrease rapidly as they approach the range of 1 to 10 THz, the so-called "terahertz gap".[1] Among the two techniques which are efficient in this frequency region, p-Ge lasers require cryogenic temperatures for continuous-wave operation which raises the cost as well as the size of the equipment. The other is difference frequency generation (DFG) by a nonlinear optical crystal, which is advantageous due to its room temperature operation and to an even broader THz output spectrum than that produced by widely used ultrafast photoconductive devices.[5,6] This suggests that the nonlinear optical (NLO) method is a potential technique for THz generation.

Materials that find attention in this field can be broadly classified into three categories, semiconductors, inorganic electro-optic crystals and organic electro-optic crystals. $LiNbO_3$ and $LiTaO_3$ are inorganic crystals having low nonlinear optical (NLO) coefficients with high dielectric constants making them less popular.[7] ZnTe, GaP, GaAs, GaSe, CdTe and InP are some of the semiconductor materials which possess large NLO coefficients compared to inorganic crystals. However, most of these materials are cubic crystals and hence, the birefringence effect is absent for phase matching which reduces the performance of difference frequency generation sources. The NLO coefficient and phase

[a] *Department of Physics, Loyola College, Chennai 600034, India*
[b] *Department of Electrical Engineering, University of Chile, Av. Tupper 2007, Santiago 8370451, Chile. E-mail: jerald.ramaclus@raig.uchile.cl, jeraldramaclus@gmail.com*
[c] *Department of Materials Science, University of Chile, Av. Tupper 2069, Santiago 8370451, Chile*

† Electronic supplementary information (ESI) available: Table of sample compositions, videos of the nucleation mechanism of samples A, B and C, simulated powder XRD patterns of pure and hydrated DAST, NMR and Raman spectra of pure DAST and sample B, face indexing of sample B, and hydrogen bonding within the unit cell of DAST. See DOI: 10.1039/c4ce02470b

matching ability are the defining factors that determine the conversion efficiency in difference frequency generation or the nonlinear optical process in general.[8]

In this scenario, dominated by semiconductors, an organic crystal DAST, has attracted much attention due to its very high NLO coefficients, namely, d_{111} = 1230 pm V^{-1}, d_{311} = 239 pm V^{-1}, d_{122} = 166 pm V^{-1}, and d_{212} = d_{221} = 135 pm V^{-1} at 800 nm. At the same time, it has a low dielectric constant making it highly suitable for THz generation.[9] In many cases, the tuning range of THz waves generated by inorganic NLO materials is limited by the material's characteristics. Thus coverage of a wide frequency range requires different source systems. On the other hand, the use of an organic NLO crystal introduces the feasibility of ultra wide tunability due to the presence of large anisotropy and birefringence.[10,11] Recently, ultra-broad band pulsed terahertz generation using a DAST crystal up to 200 THz has also been demonstrated where the high-frequency components beyond 100 THz are much stronger than conventional electro-optic crystals such as GaSe.[12]

Though DAST is considered as one of the best THz emitters, its development is limited by its crystal growth characteristics. DAST has a high tendency to undergo multi-nucleation leading to poly-crystallization and twinning which at the same time reduces the quality and size of the single crystals.[13,14] Under humid conditions, hydrated co-crystals with centrosymmetric structure are grown preventing the solvent evaporation (SE) method, which is the simplest method for crystal growth.[15] Most importantly, the final morphology of the DAST crystal when grown from methanol does not exhibit the desired faces required for efficient THz generation.[16] The d_{111} and d_{122} coefficients are the preferred largest NLO coefficients and in order to exploit these, the (100) and (010) faces are required to be aligned toward the optical axis.[17,18] However, DAST grows as a crystal from a pure methanol solution without the (100) and (010) faces.[19] Therefore, DAST crystals are mechanically modified by cutting, polishing and using other sophisticated techniques to obtain the required morphology during which, however, a lot of the expensive, purified starting substance of the growth is lost.[20–22]

In this article, we propose a simple, cost-effective method which allows pure DAST crystals to grow by a SE method directly with the desired morphology required for efficient THz generation. Additionally, it has the welcomed side-effect of reducing multi-nucleation. This is achieved using additives (crystal growth modifiers). Researchers have used additives to control the nucleation and morphology of DAST before but no significant work has been reported yet that modifies or develops a face other than the usual (100), (110), (−110), (−1−10) and (1−10) faces in the bulk crystal form.[23–28] All these reports have been demonstrated using a slow-cooling method due to the issue of hydration during growth by the SE method. Hence, the influence of additives on DAST crystal growth by the SE method remains unclear. The choice of a suitable additive for the SE method to grow a DAST crystal is of significant importance as it should have the ability to prevent hydration and also lead to the desired morphology. Oleic acid (OA) has been used as an additive to control the nucleation in several inorganic crystals due to its superior inhibiting, stabilizing and adsorption properties.[29,30] The presence of a long alkyl chain and an unsaturated double bond provides significant hydrophobicity to the material that adsorbs it; this property is particularly attractive to prevent hydrated DAST crystallization.[31] Therefore, due to its attractive properties as a crystal growth modifier, in this article, we have investigated the influence of OA on the control of the nucleation, growth and morphology of the DAST crystals grown by the SE method.

Experimental

Nucleation studies

The nucleation point of DAST in methanol with OA was measured as follows. A volume of 5 ml of a saturated solution of DAST in methanol at 20 °C was taken in a test tube and the solvent was allowed to evaporate. At the point where the first nucleation occurs, the quantity of the remaining solvent was measured and its equilibrium concentration was calculated based on the solubility curve. This process was repeated at 25 and 30 °C for three different mole ratios of DAST (M_W = 410.62 g mol^{-1}) and oleic acid (M_W = 282.46 g mol^{-1}) in methanol: 1 : 0 (sample A), 1 : 1 (sample B) and 1 : 2 (sample C). The nucleation mechanism was further investigated by casting a drop of DAST–OA–methanol solution of the three different compositions mentioned earlier on a glass slide at 25 °C. The nucleation was recorded using a CCD sensor through an optical microscope.

Crystal growth

DAST crystals were grown by the spontaneous nucleation, SE method in the absence and presence of OA as an additive. Three different solutions of DAST, methanol and OA (according to the compositions used in nucleation studies) were prepared, each in 16 ml of methanol at 20 °C (Table 1 of the ESI†). The measured quantities of DAST were first dissolved in methanol by heating and then transferred to 18 ml plastic test tubes. The solutions were allowed to cool and later the measured quantities of OA were added to each test tube, sealed and allowed to disperse through mechanical shaking for 5 hours. Then the test tubes were kept in a constant temperature bath at 21 °C for 1 day. After one day, no separation of OA was observed and it was found visually to be dispersed well in the solution. The temperature was reduced to 20 °C and the seals of the test tubes were replaced with perforated lids. In this way, the solvent was allowed to evaporate at a rate of 0.8 ml per day.

Characterization

The nucleation mechanism and etching analyses were studied by using an Olympus-BX41-LED optical microscope.

Powder X-ray diffraction analysis was performed using a Siemens P4 diffractometer in order to identify the structure. The morphology of the single crystals was investigated by using a Bruker D8 Quest single crystal X-ray diffractometer equipped with a photon 100 CMOS detector. The morphology of the DAST crystal was simulated using WinXMorph software by updating the lattice parameters and symmetry system of DAST.[32] The angle between the planes was calculated using the "calculate angle" option and by choosing the planes. The angle of the single crystal faces was also measured using a contact goniometer. The proton NMR spectrum was recorded using a Bruker Avance III 500 MHz FT-NMR spectrometer with deuterated methanol as the solvent. Raman spectra were measured using a Bruker RFS 27 standalone FT-Raman spectrometer in the spectral range of 50–4000 cm^{-1} with a Nd:YAG laser source at 1064 nm.

Results and discussion

Nucleation

It was observed that the rate of nucleation increased from sample C to sample A (Fig. 1). Hence, the metastable zone width is largest in sample C and decreased toward A. It has been reported that additives suppress the cluster formation and increase the metastable zone width resulting in fewer but larger crystals with higher quality.[29] The large metastable zone width due to the presence of OA, when compared to other additives used previously, is expected to result in larger crystals than in previous studies.[23–25] The excess OA (more than the equal ratio of DAST in sample C) has increased the critical size of the nucleus, hence crystal growth could not proceed until the nucleus reached the enhanced critical activation energy to overcome the inhibiting process. Only those nuclei which overcame the critical energy have grown into crystals and others have dissolved and transported to the growing crystal due to concentration gradients. Therefore, OA has significantly affected the nucleation.

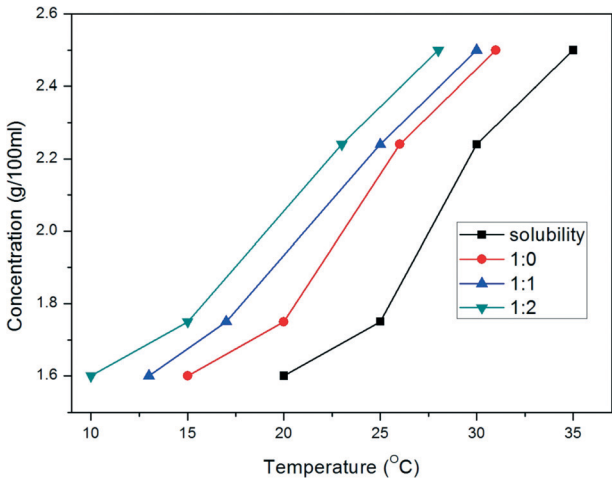

Fig. 1 Measured solubility curve of DAST in methanol. Nucleation curves of samples A, B and C.

Spherulites were observed when the nucleation mechanism was investigated on the glass slides and these studies provide more insights into the nucleation behavior of DAST in different compositions of OA in methanol. In sample A, primary and secondary nucleation could also be observed in the form of spherulites and a concentration gradient around the existing crystal, respectively (Movie 1). When these spherulites are viewed between crossed polarization filters, they exhibit the Maltese extinction cross (Fig. 2a and b) which vindicates that these are not polycrystalline aggregates.[33] It can be observed that the primary nucleation accompanies the cluster formation first and once the critical size is achieved they grow as a crystal. These clusters, which are highly disordered, are the origin of spherulite formation.[34] Once the crystal forms, the spherulites disappear because of the diminishing disorder due to the crystalline nature.

A similar mechanism to that of sample A is observed in sample B where the cluster formation and subsequent growth into crystals takes place (Movie 2). The major difference here is the pattern of the noncrystallographic branching which is a consequence of the change in characteristics of the cluster: the existence of a smaller cluster and the appearance of a partially crystalline core which exists inside the cluster (Fig. 2c and d). OA has disconnected most of the spherulites from the neighboring ones unlike in sample A where the spherulites were connected *via* the branches; this suggests that the transport of the solute to the nucleus has been affected.[35]

In the case of sample C, the nuclei are completely separated by OA and the branching from the nucleus is not as uniform as that in sample A or B (Fig. 2e and f). It appears that in this case the spherulites adopted a different branching growth mechanism (Movie 3). The formation of crystals inside the cluster suggests the possibility of a two-step nucleation mechanism inside the core of the spherulites (Fig. 2f).[36] The secondary nucleation *via* the concentration gradient is also completely affected by OA which surrounds it. The emergence of the crystal inside the cluster completely eliminates the noncrystallographic branching around the core. The suppression of cluster formation by OA is evident from the relationship between the cluster and the noncrystallographic branching associated with the spherulites observed in samples A, B and C. It is worth noting that in sample A, polycrystals appeared and samples B and C were free from such polycrystals during the nucleation studies. The longer time that samples B and C took to nucleate was recorded in videos and the observation of the suppression of cluster formation further supports the increase of the metastable zone width. This strongly suggests that OA efficiently affects the way DAST nucleates. The phenomenon observed on the glass plates cannot be suggested as the nucleation mechanism inside the solution of the growing crystal, but can be used as an indication for possible changes in the morphology due to the influence of OA on the nucleation of DAST.

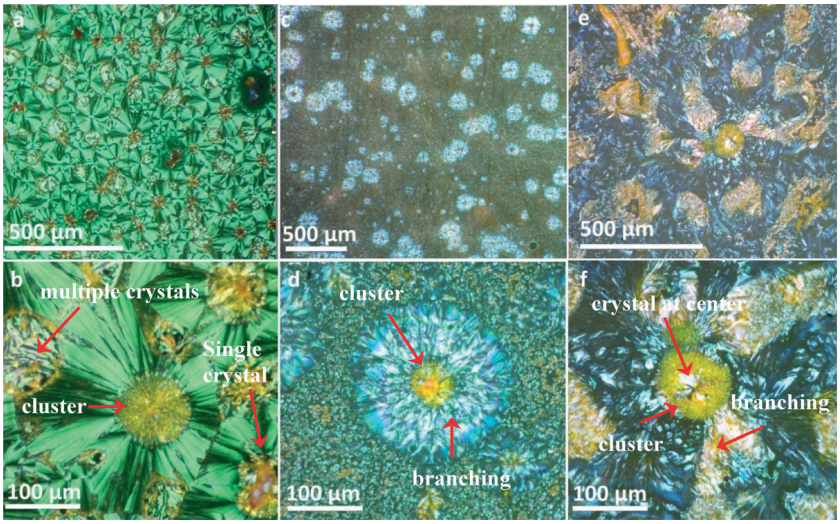

Fig. 2 Micrographs of spherulite formation in samples A (a, b), B (c, d) and C (e, f). All micrographs where taken under crossed polarization filters. Note that only sample A displays the Maltese crosses.

Single crystal characteristics

The major consequences of nucleation control and large metastable zone are the size enhancement of the crystal and morphology changes. After 20 days of growth, crystals of different sizes were obtained. At the end of the growth, when all methanol evaporated, OA settled at the bottom of the crystals and was also stuck to the crystals. In sample B most of the crystals appeared to be twinned or as polycrystals but in fact they were sticking together due to OA and could be easily separated. In appearance, samples A and C are reddish in color and are also transparent, whereas sample B has a metallic green luster and is not transparent (Fig. 3). In sample C, the largest single crystal harvested was of the size 25 × 5 × 0.5 mm^3 as shown in Fig. 3c. It can be observed that OA is an effective additive to control the nucleation and growth of DAST crystals. As the proportion of OA increased with respect to DAST, bigger crystals were obtained which directly reflects the consequence of a wider metastable zone.

Another important issue in growing DAST crystals by an evaporation method is the formation of hydrated co-crystals, and in order to investigate this, powder XRD was performed on the 001 face of the grown crystals of all samples (Fig. 4). For comparison, we have also measured the powder XRD of the finely powdered pure DAST which was annealed at 100 °C for 1 hour to remove any water molecule that might be present. From the simulated powder XRD pattern of hydrated DAST, we observe that some of the peaks coincide with those of pure DAST especially at 12° and 24° (Fig. S1†). The major difference is, a peak is observed at 6° in the case of hydrated DAST, which is absent in pure DAST. Since most of the earlier research studies reported the powder XRD patterns of DAST in the range of 10 to 40°, the possibility of hydration is overlooked in the case of SE methods.[23,27,28,37,38] Therefore,

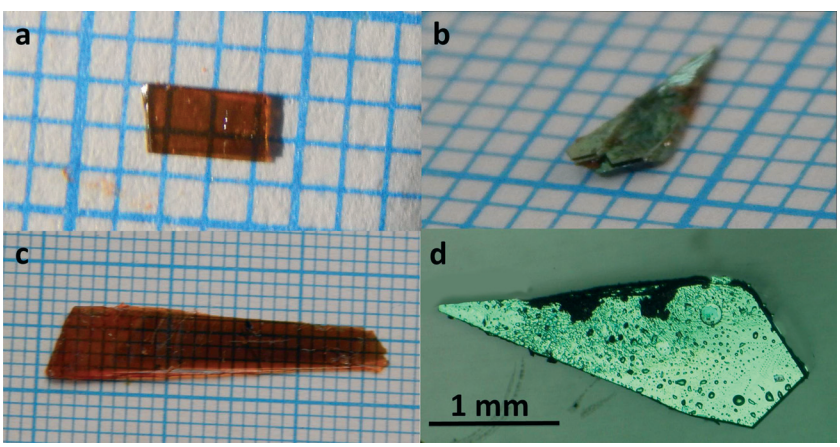

Fig. 3 DAST crystals grown using OA from samples (a) A, (b) B, and (c) C, and (d) a single crystal of sample B after separation from other crystals sticking to it.

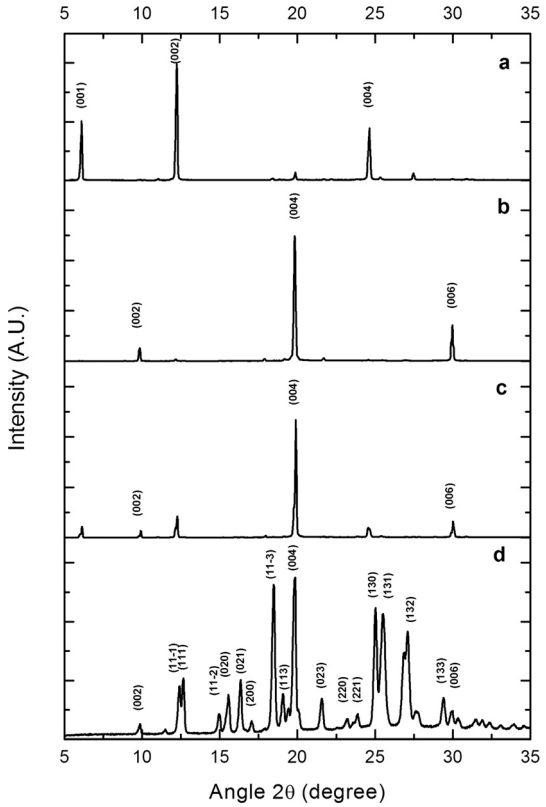

Fig. 4 Powder XRD patterns for the 001 face of (a) sample A, (b) sample B, (c) sample C and (d) pure DAST in powder form.

in order to distinguish between pure and hydrated DAST, the powder XRD has to be measured from 5° where a peak around 6° is observed only in hydrated-DAST (triclinic, $P\bar{1}$) and not in pure DAST (monoclinic *Cc*). In the case of sample A, the major peaks at 6.1°, 12.2° and 24.6° correspond to the (001), (002) and (004) planes of the triclinic space group $P\bar{1}$ (Fig. 4a and S1†) and not those of the monoclinic *Cc* crystal system (Fig. 4d).[15] The XRD pattern of sample B is found to be in good agreement with the powder XRD pattern of pure DAST and the peak around 6° is absent (Fig. 4b). Usually, DAST crystals grown from an evaporation method form hydrated co-crystals and here, the hydrophobicity of OA could have prevented such formation.[15] The powder XRD pattern of sample C possesses the characters of both forms of DAST (Fig. 4c). We can observe the peaks at 6.1°, 12.2° and 24.6°, however with a lower intensity with respect to those of pure DAST. It could be possible that the crystal is partially hydrated; the outer layers of the DAST crystal are hydrated. Further, in order to determine if OA is present as an impurity in sample B, NMR and Raman spectra were measured. In the NMR analysis, there were no major peaks other than that of DAST observed (Fig. S2–S4†).[39,40] OA has major peaks at 5.35 ppm, 1.45° to 1.23 ppm due to HC═CH, $(CH_2)_3$ and $(CH_2)_5$ hydrogens, respectively, and there is no trace of such peaks in sample B. In the case of the Raman spectrum of sample B, the peaks match perfectly with those of pure DAST. There are negligible shifts in the peaks which may be due to unknown experimental conditions. OA possesses a very strong Raman peak around 2800 cm^{-1} and its absence clearly indicates that sample B is free of OA.[41]

Crystal growth and morphology

The morphology of DAST crystals is significantly affected by the influence of OA in the case of sample B. Growth conditions like the evaporation rate and concentration also strongly affect the shape of the crystal and in the case of DAST such conditions produce either thicker or thinner crystals.[42,43] In another method, mixed solvents were used to control the thickness of the crystals which demonstrates the anisotropic growth of DAST in a preferred direction due to the interaction of different solvents.[43] Usually DAST crystals grow along the *a*–*b* plane through a slow-cooling method thus having a square platelet morphology with the (001) face as the largest surface area. The other faces that show up in the final morphology are the (110), (1–10), (–110) and (–1–10).[16] Square shaped DAST crystals are also obtained by the evaporation method but mostly they turn out to be hydrated. In few cases, hexagonal shaped DAST crystals were observed at high supersaturations as microcrystals or twinned bulk crystals (by temperature lowering and SE methods).[44,45] It is reported that the growth rates of the (100) and (010) planes were almost similar and during prolonged growth, the (020) face finally disappears in bulk crystals.[44] In the present work, in the case of sample B, we find that crystals form in an irregular hexagonal shape (Fig. 3d) with the (010) face emerging and existing in the final morphology at a supersaturation temperature of 20 °C. This is an indication of the influence of OA on DAST crystal growth. It has been reported that twinned crystals possess a flat surface with the (001) face on both sides and these crystals have an irregular hexagon shape.[45] In order to identify the faces of the largest surface of the DAST crystals grown from sample B, one crystal was subjected to single-crystal X-ray diffraction analysis. The unit cell parameters were obtained as follows: a = 10.3652(5) Å, b = 11.3225(2) Å, c = 17.8937(1) Å, β = 92.242(2)° and V = 2100.00(4) (Å^3) with the monoclinic *Cc* space group, which is in good agreement with the literature.[19] Once the unit cell parameters and orientation matrix were obtained, face indexing was performed which revealed that one of the flat surfaces is (001) and the other is $(00\bar{1})$ (Fig. S5†). This confirms that the crystals are not twinned and the hexagonal shape is not a consequence of twinning. Therefore, we find that this change in shape is not due to the factors observed in the earlier literature.

The existence of the (010) face in the grown crystal was further confirmed by measuring the interfacial angle between the planes by a contact goniometer. The measured angles of 95° between the $(1\ \bar{1}0)$ and (110) faces and 135° between the $(1\ \bar{1}0)$ and (010) faces are found to be close to the values simulated for the DAST crystal system (95.1° and 135.45°) (Fig. 5). It was found that the (010) face did not grow completely in sample B. This incomplete growth of the crystal is attributed to the depletion of the solute at the end of the

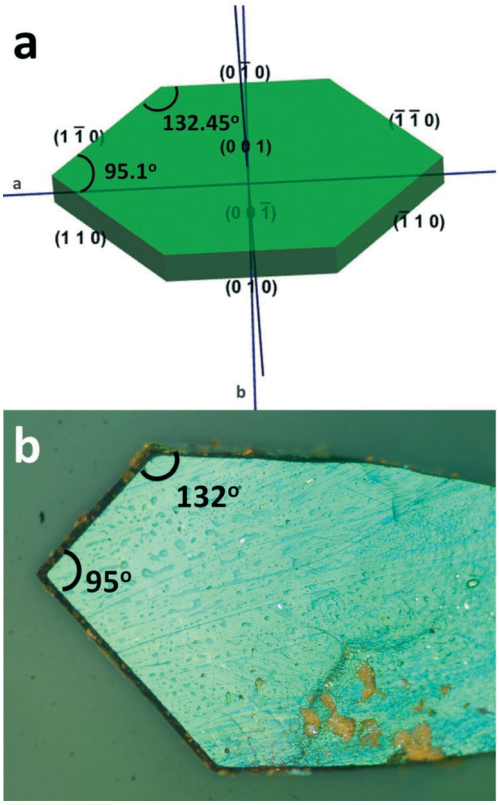

Fig. 5 (a) Simulated morphology of the DAST crystal system with the calculated interfacial angles. (b) Measured interfacial angles of the DAST crystal grown from sample B.

growth (Fig. 3d). When the surface of sample B was etched with methanol for 10 s, it revealed a 2-dimensional growth mechanism which is hexagonal with (010) as the major face (Fig. 6a and b). In order to confirm that it is OA that is responsible for such a pattern, we also used the composition of OA in methanol according to sample B and etched the surface of the pure DAST crystal grown from methanol. The etch patterns are incomplete hexagons which is evident from Fig. 6c. When a similar pure DAST crystal was etched with methanol (no OA) for the same duration we did not observe a hexagonal etch pattern (Fig. 6b) but instead a typical pattern (Fig. 6d) as reported earlier for DAST.[25] Therefore, it becomes evident that it is OA which inhibits the growth on the (010) direction directly through the interaction with DAST.

The possible roles of OA in the DAST–methanol solution are: (i) as a dimer due to the hydrogen bonding interaction with the solvent, (ii) de-protonation of OA due to the ionic nature of DAST and (iii) the interaction of hydrogen bonding with the anion of DAST. It has been reported that, when OA is used as an additive in a polar solvent, it has the tendency to form dimers due to the hydrogen bonding interaction with the solvent.[46] Apart from that, the carboxyl hydrogen atom of oleic acid could also form a bond with the hydroxyl group of methanol.[47] Therefore, these reports suggest that the hydroxyl group of OA has a strong tendency to form a hydrogen bond with any molecule. If OA would be deprotonated, it would affect, when attached to the crystal, the van der Waals forces and hydrogen bonds between the cations and that of the anions resulting in a hindrance along the *a*-axis. However, the (100) face has not emerged which reveals that deprotonation did not occur and also, since OA is not an ionic molecule, it is highly unlikely. The observation from the spherulite growth reveals that OA has affected the branching; OA has inhibited the interaction of methanol with DAST molecules. Since methanol molecules are involved in the dissolution of DAST ions, they are less likely to form

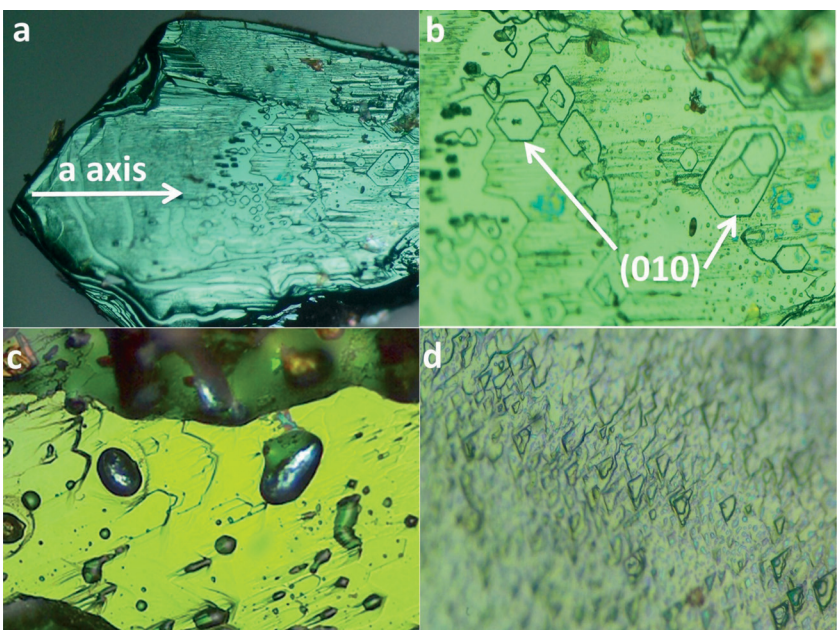

Fig. 6 (a) Etching of sample B with methanol, (b) magnified image of Fig. (a), (c) etching of pure DAST with methanol–OA and (d) etching of a pure DAST crystal with methanol.

hydrogen bonds with OA. The emergence of the (010) face clearly vindicates the interaction of the hydroxyl group of OA and oxygen of the DAST anions, as the (010) surface exposes these oxygen atoms to the solution and OA, resulting in an inhibited growth along the *b*-axis.

It is known that the hydrogen bondings between the oxygens of the tosylate anions and the hydrogens of the olefin- and benzene-parts play a vital role in packing the DAST molecules in a parallel alignment and stacking them along the *b*-axis. Follonier *et al.* reported that adjacent cation molecules are bound by van der Waals forces between the donor of one molecule and the acceptor of the next-lying molecule, which is responsible for the growth along the *a*-axis.[48] The strongest hydrogen bonds (2.636 Å) between two adjacent tosylates in the DAST crystal along the *b*-axis are the major binding forces driving the growth along that direction (Fig. S6†). The other strong hydrogen bonds between the CH– atoms of the cations and –OS groups of the anions with distances of alternately 2.615 and 2.454 Å are responsible for the parallel alignment of the cation molecules. It is evident from the structure that the hydrogen bonds between the anions are also responsible for the growth along the *b*-axis and OA has interacted with this hydrogen bonding so that the growth along the *b*-axis is hindered (Fig. 7). We can summarize these findings as follows. (i) When there is no OA, the DAST crystal grows along the *a*- and *b*-axes at the same rate; (ii) when OA is present at an equal ratio to that of DAST, the growth rate along the *b*-axis slows down significantly with respect to that of the *a*-axis; and (iii) when excess OA is present, the growth along the *b*-axis slows down but not as significantly as in the previous case. While we have shown in this paper the enhancement of the (010) face, it may also be possible to develop the (100) face by using an appropriate combination of additives which can be tried in the future.

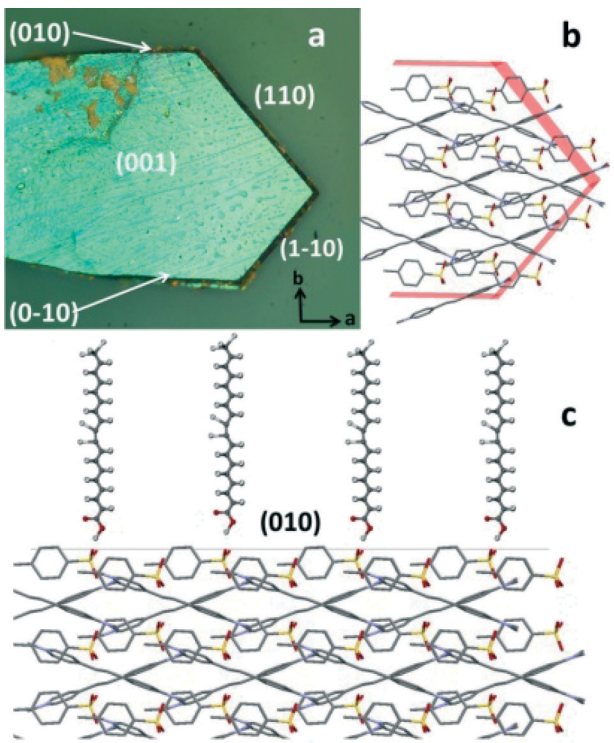

Fig. 7 (a) Morphology of DAST crystals belonging to sample B, (b) packing of DAST molecules in sample B and (c) possible interaction of OA with the (010) face of the DAST crystal.

Conclusion

Nucleation studies reveal the two step mechanism adopted by DAST molecules to grow into a single crystal. The spherulite patterns of different compositions reveal how OA reduces the cluster formation during the nucleation of DAST crystals. Although several additives have been used previously, for the first time the (010) face of the DAST crystal is successfully developed by employing OA as an additive during the growth of the crystal. Apart from the morphology, the size of the crystals also increased considerably when compared to other methods reported previously. Moreover, this method is cost-effective as it reduces the quantity of DAST required to grow suitable crystal sizes for THz applications.

Acknowledgements

The authors would like to thank Dr. Mauricio Fuentealba, Laboratorio de Química Inorgánica, Instituto de Química, Pontificia Universidad Católica de Valparaíso, Valparaíso, Chile, for performing single crystal XRD analysis. This work was partially supported by CONICYT-ALMA, project number 31110014.

References

1 M. Tonouchi, *Nat. Photonics*, 2007, **1**, 97.
2 A. Wootten and A. R. Thompson, *Proc. IEEE*, 2009, **97**, 1463.
3 D. Arnone, *MIT Technology Review*, 2004, vol. 32, p. 6.
4 B. Ferguson and X. C. Zhang, *Nat. Mater.*, 2002, **1**, 26.
5 P. H. Siegel, *IEEE Trans. Microwave Theory Tech.*, 2002, **50**, 910.
6 C. M. Armstrong, *IEEE Spectrum*, 2012, **49**, 36.
7 I. Wilke and S. Sengupta, *Nonlinear Optical Techniques for Terahertz Pulse Generation and Detection—Optical Rectification and Electrooptic Sampling, Terahertz Spectroscopy: Principles and Applications*, ed. S. L. Dexheimer, CRC Press, 2007, p. 42.
8 M. G. Krishna, S. D. Kshirsagar and S. P. Tewari, *Terahertz Emitters, Detectors and Sensors: Current Status and Future Prospects, Photodetectors*, ed. Dr. S. Gateva, ISBN: 978-953-51-0358-5, InTech, 2012.
9 M. Jazbinsek, L. Mutter and P. Gunter, *IEEE J. Sel. Top. Quantum Electron.*, 2008, **5**, 1298.
10 X. Zheng, C. V. McLaughlin, P. Cunningham and L. M. Hayden, *J. Nanoelectron. Optoelectron.*, 2007, **2**, 58.
11 K. Miyamoto, S. Ohno, M. Fujiwara, H. Minamide, H. Hashimoto and H. Ito, *Opt. Express*, 2009, **17**, 14832.
12 I. Katayama, R. Akai, M. Bito, H. Shimosato, K. Miyamoto, H. Ito and M. Ashida, *Appl. Phys. Lett.*, 2010, **97**, 021105.

13 M. Yusuke, T. Yoshinori, I. Takashi, Y. Masashi, Y. Yoke Khin and S. Takatomo, *Jpn. J. Appl. Phys.*, 2000, **39**, L1006.
14 H. Adachi, Y. Takahashi, J. Yabuzaki, Y. Mori and T. Sasaki, *J. Cryst. Growth*, 1999, **198–199**, 568.
15 S. R. Marder, J. W. Perry and C. P. Yakymyshyn, *Chem. Mater.*, 1994, **6**, 1137.
16 B. Ruiz, M. Jazbinsek and P. Günter, *Cryst. Growth Des.*, 2008, **8**, 4173.
17 U. Meier, M. Bosch, C. Bosshard, F. Pan and P. Gunter, *J. Appl. Phys.*, 1998, **83**, 3486.
18 A. Schneider, M. Neis, M. Stillhart, B. Ruiz, R. U. A. Khan and P. Günter, *J. Opt. Soc. Am. B*, 2006, **23**, 1822.
19 F. Pan, M. S. Wong, C. Bosshard and P. Günter, *Adv. Mater.*, 1996, **8**, 592.
20 Y. Namba, M. Tsukahara, A. Fushiki, K. Soizu and H. Ito, *Proc. SPIE*, 2003, **5180**, 55.
21 T. Kaino, B. Cai and K. Takayama, *Adv. Funct. Mater.*, 2002, **12**, 599.
22 F. Pan, K. McCallion and M. Chiappetta, *Appl. Phys. Lett.*, 1999, **74**, 492.
23 A. S. Haja Hameed, W. C. Yu, C. Y. Tai and C. W. Lan, *J. Cryst. Growth*, 2006, **292**, 510.
24 A. S. Haja Hameed, S. Rohani, W. C. Yu, C. Y. Tai and C. W. Lan, *Mater. Chem. Phys.*, 2007, **102**, 60.
25 Z. Sun, T. Chen, J. Luo and M. Hong, *J. Cryst. Growth*, 2011, **328**, 89.
26 J. I. Wu, R. Gopalakrishnan, C. I. D. Tai and C. W. Lan, *Jpn. J. Appl. Phys., Part 1*, 2004, **43**, 1507.
27 K. Kumar, R. N. Rai and S. B. Rai, *Appl. Phys. B: Lasers Opt.*, 2009, **96**, 85.
28 C. Karthikeyan, A. S. Haja Hameed, J. Sagaya, A. Nisha and G. Ravi, *Spectrochim. Acta, Part A*, 2013, **115**, 667.
29 W. Bu, Z. Chen, F. Chen and J. Shi, *J. Phys. Chem. C*, 2009, **113**, 12176.
30 X. Liang, L. Gao, S. Yang and J. Sun, *Adv. Mater.*, 2009, **21**, 2068.
31 N. Patra, M. Salerno, A. Diaspro and A. Athanassiou, *Microelectron. Eng.*, 2011, **88**, 1849.
32 W. Kaminsky, *J. Appl. Crystallogr.*, 2005, **38**, 566.
33 A. G. Shtukenberg, Y. O. Punin, E. Gunn and B. Kahr, *Chem. Rev.*, 2011, **112**, 1805.
34 L. Gránásy, T. Pusztai, G. Tegze, J. A. Warren and J. F. Douglas, *Phys. Rev. E: Stat., Nonlinear, Soft Matter Phys.*, 2005, **72**, 011605.
35 A. A. Chernov, *J. Cryst. Growth*, 1999, **196**, 524.
36 P. G. Vekilov, *J. Cryst. Growth*, 2005, **275**, 65.
37 R. Jerald Vijay, N. Melikechi, T. Rajesh Kumar, J. G. M. Jesudurai and P. Sagayaraj, *J. Cryst. Growth*, 2010, **312**, 420.
38 K. Jagannathan, S. Kalainathan, T. Gnanasekaran, N. Vijayan and G. Bhagavannarayana, *Cryst. Growth Des.*, 2007, **7**, 859.
39 R. J. Vijay, N. Melikechi, T. Thomas, R. Gunaseelan, M. A. Arockiaraj and P. Sagayaraj, *Mater. Chem. Phys.*, 2012, **132**, 610.
40 T. Vijayakumar, I. Hubert Joe, C. P. Reghunadhan Nair, M. Jazbinsek and V. S. Jayakumar, *J. Raman Spectrosc.*, 2009, **40**, 52.
41 P. Tandon, G. Förster, R. Neubert and S. Wartewig, *J. Mol. Struct.*, 2000, **524**, 201.
42 K. Nagaoka, H. Adachi, S. Brahadeeswaran, T. Higo, M. Takagi, M. Yoshimura, Y. Mori and T. Sasaki, *Jpn. J. Appl. Phys.*, 2004, **43**, L261.
43 T. Matsukawa, M. Yoshimura, Y. Takahashi, Y. Takemoto, K. Takeya, I. Kawayama, S. Okada, M. Tonouchi, Y. Kitaoka, Y. Mori and T. Sasaki, *Jpn. J. Appl. Phys.*, 2010, **49**, 0755021.
44 A. S. Haja Hameed, W. C. Yu, Z. B. Chen, C. Y. Tai and C. W. Lan, *J. Cryst. Growth*, 2005, **282**, 117.
45 S. Brahadeeswaran, S. Onduka, M. Takagi, Y. Takahashi, H. Adachi, T. Kamimura, M. Yoshimura, Y. Mori, K. Yoshida and T. Sasaki, *Cryst. Growth Des.*, 2006, **6**, 2463.
46 W. Bu, Z. Chen, F. Chen and J. Shi, *J. Phys. Chem. C*, 2009, **113**, 12176.
47 C. W. Hoerr and H. J. Harwood, *J. Phys. Chem.*, 1952, **56**, 1068.
48 S. Follonier, M. Fierz, I. Biaggio, U. Meier, C. Bosshard and P. Günter, *J. Opt. Soc. Am. B*, 2002, **19**, 1990.

